J Biol Phys (2006) 32: 191–208
DOI 10.1007/s10867-006-9012-1

RESEARCH PAPER

Unraveling Cell Processes: Interference Imaging Interwoven with Data Analysis

N.A. Brazhe · A.R. Brazhe · A.N. Pavlov · L.A. Erokhova · A.I. Yusipovich · G.V. Maksimov · E. Mosekilde · O.V. Sosnovtseva

Received: 10 February 2006 / Accepted: 20 March 2006 /
Published online: 11 November 2006

Abstract The paper presents results on the application of interference microscopy and wavelet-analysis for cell visualization and studies of cell dynamics. We demonstrate that interference imaging of erythrocytes can reveal reorganization of the cytoskeleton and inhomogenity in the distribution of hemoglobin, and that interference imaging of neurons can show intracellular compartmentalization and submembrane structures. We investigate temporal and spatial variations of the refractive index for

N. A. Brazhe (✉) · A. R. Brazhe · L. A. Erokhova · A. I. Yusipovich · G. V. Maksimov
Biophysics Department, Biological Faculty, Moscow State University,
Vorobievy gory 1, Building 12, 119992 Moscow, Russia
e-mail: una@biophys.msu.ru

A. R. Brazhe
e-mail: brazhe@biophys.msu.ru

L. A. Erokhova
e-mail: erokhova@yahoo.com

A. I. Yusipovich
e-mail: yavor@pisem.net

G. V. Maksimov
e-mail: maxim@biophys.msu.ru

A. N. Pavlov
Physics Department, Saratov State University,
Astrakhanskaya Street 83, 410026 Saratov, Russia
e-mail: pavlov@chaos.ssu.runnet.ru

E. Mosekilde · O. V. Sosnovtseva
Department of Physics, The Technical University of Denmark,
2800 Kongens Lyngby, Denmark

E. Mosekilde
e-mail: erik.mosekilde@fysik.dtu.dk

O. V. Sosnovtseva
e-mail: olga@fysik.dtu.dk

different cell types: isolated neurons, mast cells and erythrocytes. We show that the refractive dynamical properties differ from cell type to cell type and depend on the cellular compartment. Our results suggest that low frequency variations (0.1–0.6 Hz) result from plasma membrane processes and that higher frequency variations (20–26 Hz) are related to the movement of vesicles. Using double-wavelet analysis, we study the modulation of the 1 Hz rhythm in neurons and reveal its changes under depolarization and hyperpolarization of the plasma membrane. We conclude that interference microscopy combined with wavelet analysis is a useful technique for non-invasive cell studies, cell visualization, and investigation of plasma membrane properties.

Key words interference microscopy · double-wavelet analysis · cell imaging · cell dynamics · neurons

Abbreviations

IOP intrinsic optic properties
RI refractive index

1 Introduction

Cells exhibit dynamical processes over a broad range of time-scales and occurring in a variety of cellular compartments. The response of a cell to external stimuli involves both the plasma membrane and different organelles and may cause changes in the cellular shape and volume as well as in the intracellular compartmentalization. Investigation of the relations between the cellular processes can contribute towards a better understanding both of normal cellular functions and of various pathological states. This requires a combination of advanced methods of biological experimentation with new approaches in data-series analysis. Traditional electrophysiological and fluorescence microscopical methods are more or less invasive and can influence the very cellular processes they are designed to study. It is therefore essential to find noninvasive probes to study cellular activity.

Reorganization in the plasma membrane, relocations of organelles, and changes in the composition and ionic concentrations of the cytoplasm can change the intrinsic optic properties (IOP) and the local refractive index (RI) of the cell. The possibility of using IOP as a noninvasive probe for neurons was first considered by Hill and Keynes [1, 2]. They observed changes in the light scattering intensity from a nerve during electrical activity. Cohen [3] found that the intrinsic optical signals depend on the ion currents through the membrane and on the membrane potential. Stepnoski [4] showed that the intensity of light scattered by the mollusc *Aplysia* neurons depends linearly on the transmembrane potential. It is now clear that the optical properties of the cell (e.g., refractive index) depend not only on the cellular electric activity and ion fluxes but also on the cell volume and shape, and on the location of organelles [5]. It is generally considered, however, that changes in the refractive index mainly relate to events in the plasma membrane. Since the processes in the plasma membrane are more pronounced in neurons as compared with other types of cells, they have been chosen as the most appropriate object for the detection of

the intrinsic optic signals. During the last few years, the detection of the intrinsic optic properties has become a quite popular technique for non-invasive studies of neuron electrical activity. Standard and functional coherence tomography, based on measurements of light scattering intensity, have been applied for visualization of neural tissue morphology and detection of optical changes during electrical excitation [6, 7]. There are certain difficulties associated with the registration of light scattering. Stepnoski and Kleinfeld noticed that intrinsic optic signals are relatively small compared to practical detection limits and difficult to observe without extensive signal averaging [4, 8]. Interference microscopy represents an alternative measurement technique that incorporates phase conjugate optics to compensate for distortions in the optical wavefront that are induced by the preparation. Interference microscopy provides information about the spatial variation of the refractive index in dependence of the plasma membrane processes and cytoplasm structure. Hence, using highly sensitive detectors and carrying out the measurements of the local refractive index it is possible to describe cellular processes and compartmentalization. Until now only nerve cells have been used for studies of intrinsic optic signals. In the present paper we show how laser interference microscopy can be used for investigations of the optic properties of different cell types.

Temporal measurement of an optic signal from a specific point gives information about the dynamics of the refractive index [9, 10]. Conventional techniques of data-series analysis (e.g., Fourier transform) and statistics have limited resolution to study cellular signals that are typically nonstationary and inhomogeneous. Part of this nonstationarity may be ascribed to changing environmental conditions or to interacting regulatory processes. It is known, however, that the degree of nonstationarity can differ between healthy and diseased states [11]. Because of their nonstationarity, the analysis of physiological time series often applies the concept of slowly varying parameters. Here, it is assumed that the statistical characteristics of the data remain practically constant during certain time intervals, and the analysis is performed by using a sliding window. This approach is useful if the nonstationarity is associated with low-frequency spectral components in relation to the physiological rhythms of interest. If the properties of the experimental data display essential variations over short time intervals, one has to apply specialized tools such as wavelet analysis [12–14], detrended fluctuation analysis [17], or other techniques [18].

Biological time series often demonstrate the coexistence of several different oscillatory components. At the cellular level, for instance, different types of nerve cells exhibit complex patterns of fast and slow rhythms in their bursting dynamics [19], and pancreatic β-cells display simultaneous oscillations of electrophysiological and metabolic origin [20].

A first step in the analysis is to separate the slow and the fast oscillatory modes. A way to approach this is to apply band-pass filtering, although in nonlinear systems this procedure may fail to correctly separate the different modes in the presence of harmonics or sum and difference frequencies in the spectrum. In particular, if the instantaneous frequency of a mode changes in time, the choice of filter parameters becomes a matter of concern. On one hand, one cannot apply a narrow frequency range for filtering because the rhythms drift. On the other hand, if the two modes are close enough in the frequency domain, one cannot use a broad frequency range in the band-pass filter since in that case the rhythms may not be separated. Such problems can sometimes be solved by using a sliding-window analysis [21] or, as we

shall demonstrate below, different aspects of multimode dynamics can be studied with wavelets.

Multimode dynamics could result from a purely linear superposition of independent oscillatory components. In most cases of biological interest, however, some kind of coupling is likely to exist between the various processes, causing them to adjust their dynamics relative to one another. Nonlinear interactions can give rise to a number of interesting phenomena including chaos, synchronization and modulation. None of these phenomena, which can be of significance both to normal physiological regulation and to the development of various diseases, occur in linear systems. Nonlinear interactions can be studied by means of bispectrum analysis [22] or wavelet-based techniques [23]. Nonlinear interactions often lead to the universal phenomenon of synchronization [24, 25]. In many cases, however, an obvious synchronization cannot be observed while modulation of one mode in the presence of another mode takes place [26]. Such situations arise, for instance, if the coupling is relatively weak as measured by the rigidity of the internal dynamics of the interacting oscillators, if the frequencies of the oscillators are too different, and/or if the system is influenced by too many disturbing factors to allow it to settle down into a particular state of synchronization.

In this paper we demonstrate the results of cell imaging and cell dynamics *via* the combination of interference microscopy and data analysis based on the wavelet transformation.

2 Cell Imaging

2.1 Method of the Laser Interference Microscopy

2.1.1 Experimental Technique

Laser interference microscopy is based on the measurement of the local phase shifts of the laser beam transmitted through an object [27–29]. Figure 1 illustrates the principle of the interference microscope. The reference beam, reflected from the control mirror, and the beam, transmitted through the object and reflected from the bottom mirror layer, interfere on the detector where the optic path difference between the two beams is estimated. This measured value is normalized to the wavelength in order to obtain the so-called phase height of the object Φ at a particular point:

$$\Phi = \frac{\phi_0 - \phi_{obj}}{2\pi} \cdot \frac{\lambda}{2} - \Phi_0. \tag{1}$$

Here ϕ_0 and λ are the initial phase and the wavelength of the laser beam, respectively, ϕ_{obj} denotes the phase in the presence of the object, and Φ_0 is a constant phase shift determined by the choice of phase reference point. Phase height values $\Phi(x, y)$ at all points of the object form a phase height relief (or interference image) of the cell.

As discussed in the introduction, the phase height depends on the spatial distribution of the refractive index inside the cell and on geometrical cellular sizes and

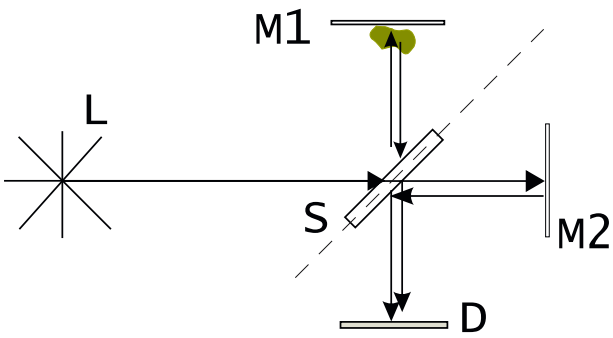

Figure 1 The principle of the interference microscope. The laser (L) beam is divided on the beam splitter S. The reference beam reflects from the control mirror M2 and the object beam transmits through the object and reflects from the mirror M1. On the detector D, the beams interfere and form an interference image of the object.

shapes. For objects that are homogeneous in the direction of the light beam, the phase height can be defined as

$$\Phi(x, y) = (n_{obj} - n_s)Z - \Phi_0 \tag{2}$$

where n_{obj} and n_s are the refractive indices of the cell and of the physiological saline, respectively. Z is the geometrical height of the studied volume. Thus, if we know n_s and n_{obj} we can measure Φ and in this way determine the precise cellular volume. Most cells are heterogeneous objects. In this case the phase height is

$$\Phi(x, y) = \int_0^Z (n_{obj}(x, y, z) - n_s)\mathrm{d}z - \Phi_0 \tag{3}$$

with n_s being the (constant) refractive index of the physiological saline and $n_{obj}(x, y, z)$ the refractive index of the cell at a point (x, y) a distance z from the mirror. Z is the upper limit of integration that is chosen as the point above the cell. The lateral resolution of the method depends on the laser wavelength (λ) and the numerical aperture (NA) according to the Abbe formula [30]:

$$D \approx 0.61\lambda / NA \tag{4}$$

and is, obviously, better for shorter wavelengths. In this work we use an objective with an aperture of $NA = 0.15$. The wavelength of the laser is $\lambda = 532$ nm and, thus, $D = 2.16\ \mu$m.

2.1.2 Experimental Procedure

Experiments were carried out on the modulation interference microscope MIM 2.1 developed by the company 'Amphora Laboratories' (Russia) [31–33]. MIM 2.1 is based on the 'Linnik' interferometer with a laser power per cell of less than 1 mW. In order to decrease the external artificial effects a firm construction of the interferometer block, a two-level system of vibroisolation, and a channel for the substraction of artificial low-frequency vibrations are used.

Human erythrocytes, rat mast cells and isolated neurons of the pond snail *Lymnaea stagnalis* and the medicinal leech *Hirudo medicinalis* were chosen as samples. Erythrocytes were taken from the blood of healthy donors and from patients who had suffered a heart failure. These experiments were performed in accordance with the standards of the Ethics Committee of the A.L. Myasnikov Institute of Clinical Car-

diology. Mast cells were isolated from male Wistar rats as described by Graevskaya *et al.* [34]. Preparation of the pond snail and leech ganglia neurons were performed according to the procedure described in [10, 33, 35]. During the experiments, cells were placed in a containment chamber with a mirror bottom layer and with the following physiological solutions: buffer for erythrocytes (mM: 145 NaCl, 5 KCl, 1 $CaCl_2$, 1 $MgSO_4$, 4 Na_2HPO_4, 1 NaH_2PO_4, 10 glucose, pH 7.4), physiological solutions for rat mast cells (mM: 144 NaCl, 2.7 KCl, 4.6 Na_2HPO_4, 2 KH_2PO_4 with addition of 100 mg of albumin, 0.5 ml of 1 M glucose solution and 0.1 ml of 1 M $CaCl_2$ solution before experiment) and physiological solutions for snail (mM: 50 NaCl, 1.5 KCl, 4 $CaCl_2$, 1 $MgCl_2$, 11 HEPES, pH 7.5) and leech (mM: 150 NaCl, 4 KCl, 1.8 $CaCl_2$, 1 $MgCl_2$, 11 HEPES, pH 7.4). In the experiments with snail neurons we obtained phase height images and then exchanged the standard snail solution for a solution with high K^+ concentration (mM: 31.5 NaCl, 20 KCl, 4 $CaCl_2$, 1 $MgCl_2$, 11 HEPES, pH 7.5). In the experiments with leech neurons we used solution with high K^+ concentration (mM: 124 NaCl, 30 KCl, 1.8 $CaCl_2$, 1 $MgCl_2$, 11 HEPES, pH 7.4) and standard solution with valinomycin (ultimate concentration of valinomycin in the chamber was 1 μM). In order to avoid photodamage cells should be tested for the laser light effect. We have found that snail and leech neurons and mast cells absorb weakly (or do not absorb) in the region of the laser light (532 nm) and concluded that their photodamage is minimal. Laser light did not cause lysis of any of the studied cells. All experiments were performed at room temperature.

The interference working field was 27 × 27 μm, and the scanning rate was 500 pix/s. Figure 2 presents an optic photograph (a), the phase height image (b) and the phase height profile of a leech neuron (c). After isolation, leech neurons have a smooth shape, and the phase height relief reflects the location of various organelles, the cytoskeleton and different plasma membrane structures. The highest (white) points in the phase height relief indicate the highest optical density. The phase height images give information about intracellular compartmentalization and reorganization of the cytoplasm and plasma membrane that can hardly be observed by any other technique. Systematic changes of the neuron phase height provide data on the dynamics of the local refractive index resulting from the regular processes in the plasma membrane and inside the cell. Data-series (wavelet) analysis helps to reveal characteristic frequencies of these cellular processes. Data acquisition was performed by means of horizontal scans of 8 points in the phase height image. The recording points were

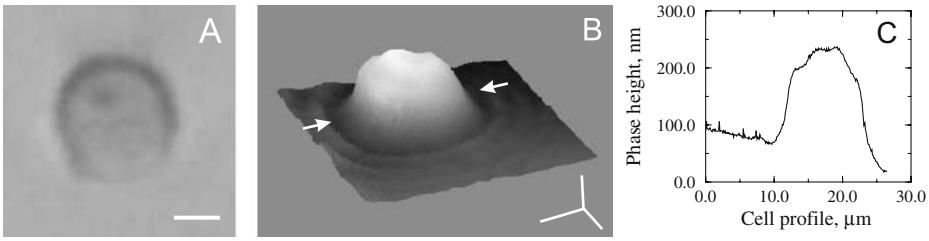

Figure 2 Optical photograph (**a**) and the phase height image (**b**) of an isolated medicinal leech neuron. *Horizontal bars* indicate the geometrical size (5 μm) and the *vertical bar* shows the phase height (100 nm). (**c**) is the phase height profile along the cell. *White arrows* in (**b**) indicate the profile position.

uniformly distributed along the scan-line (ensured by the microscope software). The scan length for dynamical studies was 5.2 μm. The sampling interval for individual point was 16 ms. In order to compare the refractive index dynamics for various cells and in the different cellular regions we performed measurements for erythrocytes, mast cells and neurons in the membrane and submembrane region (at every 0.6 μm starting from the cell boundary till 1.2 μm from the cell boundary), cell center (defined as all points at a distance greater than 2.5 μm from the cell boundary) and in the nucleus region (only for mast cells). For statistical analysis we performed 10–20 measurements in each cellular region.

2.2 Cell Visualization

Let us represent the results of the visualization by interference microscopy of two different types of cells: erythrocytes and neurons. Erythrocytes can be regarded as 'tough' cells due to their strong submembrane cytoskeleton. They have a simple intracellular structure, and their refractive index is determined by the distribution of hemoglobin and of the cytoskeleton net. On the contrary, neurons are 'soft' cells with complicated cytoplasmic compartmentalization. Isolated leech and snail neurons have round shapes without axons/dendrites. This facilitates analysis of their phase height images.

Figure 3 shows typical optical photograph (a) and phase height image (b) of an erythrocyte from the blood of a healthy donor. It has the shape of a normal erythrocyte: a discocyte. The typical toroidal form is clearly seen on the phase height image. The discocyte has a smooth shape (also seen from the optical photograph) and a homogeneous distribution of the refractive index, indicating a uniform hemoglobin distribution. On the contrary, the phase height image of the erythrocyte of the patient with heart failure (Figure 4b) has a rough toroidal form with protuberances. It is worth noticing that such structures cannot be detected from the optical photograph (Figure 4a) which appears similar to the erythrocyte of the healthy person (Figure 3a). The observed protuberanced toroidal structure can result from complex changes of cytoskeletal structure or from a nonhomogeneous distribution of hemoglobin in the cytoplasm and in the submembrane region. We suppose that the changes are caused by pathological processes in the erythrocytes or in the cardiovascular system as a whole in connection with the heart failure. Indeed, there is evidence to suggest that severe hypoxia and blood system diseases affect plasma membrane fluidity and hemoglobin properties of erythrocytes [36, 37]. All the observed changes may relate to an inhomogeneous hemoglobin distribution in the erythrocytes. However, another explanation is that the protuberanced toroidal form results from the initial phase of the discocyte transformation into echynocytes or stomatocytes. This

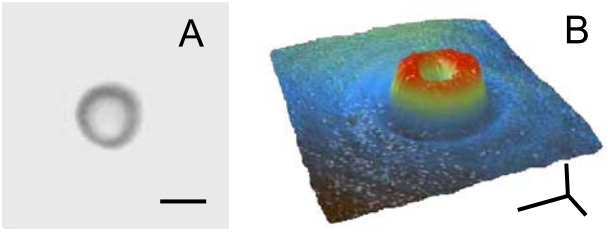

Figure 3 Optical photograph (**a**) and phase height image (**b**) of an erythrocyte from the blood of a healthy person. *x* and *y* bars indicate the geometrical size (10 μm) and the *z* bar is the phase height (100 nm).

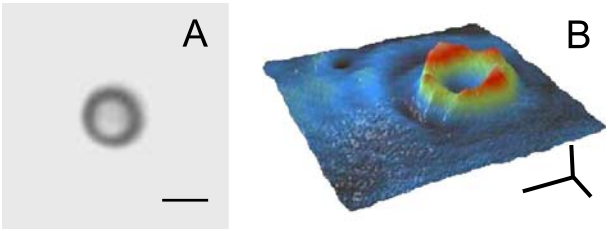

Figure 4 Optical photograph (**a**) and phase height image (**b**) of an erythrocyte from the blood of a patient with heart failure. *x* and *y* bars indicate the geometrical size (10 μm) and the *z* bar is the phase height (100 nm).

process occurs in all discocytes before their lysis but can be more easily observed in blood from non-healthy persons since more discocytes have transformed into other forms.

Our next experiment served to explore phase height images of neurons in different functional states. Figure 5 shows phase height images of the pond snail neuron in normal physiological solution (a) and in a solution with high K^+ concentration (b). It can be seen that in the high K^+ medium, the neuron's phase height has a different relief than in the normal solution. There is no difference, however, between the optical photographs (not shown here) of neurons in these two solutions. As mentioned above, snail neurons have a round shape and unsmoothed phase height profiles which are caused by variations of the local refractive index. We suppose that these variations are a result of complex processes triggered in the plasma membrane and cytoplasm. Thus, solutions with high K^+ concentration produce depolarization of the plasma membrane, short-term activation of Na^+ and Ca^{2+}-channels, and prolonged activation of the Na/Ca-exchanger [38]. Influx of Ca^{2+} into the cytoplasm causes an increase in the amount of Ca^{2+} that affects various enzymes, signaling pathways and cytoskeletal structure [39, 40]. This results in complex reorganizations of the cytoplasm and in changes of the local refractive index [5].

3 Cellular Dynamics

Cellular activity involves a multitude of processes occurring in different compartments. Many of these changes are interrelated and depend on each other. It is clear that modification of the plasma membrane structures, cytoplasm compartmentalization, position and shape of organelles alter the local refractive index. Regular cooperative processes inside the cell result in regular changes of the refractive index. Analysis of the refractive index dynamics provides information about the frequencies

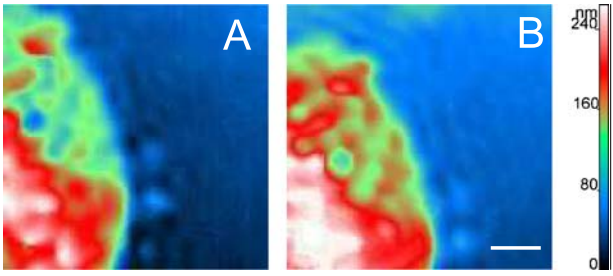

Figure 5 Phase height images of an isolated pond snail neuron under normal conditions (**a**) and in a physiological solution with high K^+ concentration (**b**).

of the various cellular processes. Thus, the combination of interference microscopy with advanced data-series analysis can be applied to study multimode dynamical phenomena in cells.

3.1 Regular Cell Activity

3.1.1 Wavelet Analysis

Spectral analysis of biological time series are often based on the application of a wavelet transformation [12, 14]. The advantages of this approach in comparison with the classical Fourier transform have been widely discussed. The wavelet transform of a signal $x(t)$ is obtained as follows:

$$T_x(a,t) = \frac{1}{\sqrt{a}} \int_{-\infty}^{\infty} x(u)\psi^* \left(\frac{u-t}{a} \right) du. \tag{5}$$

Here ψ is a 'mother' function that should be soliton-like with zero average. $T_x(a,t)$ are the wavelet coefficients and a is a time scale parameter. The details of this transform (e.g., the choice of ψ) depend on the problem to be solved. In the analysis of rhythmic components, the *Morlet* function is typically considered. Instead of the Morlet wavelet, some authors [15, 16] prefer to use other complex wavelet functions because of possible spurious effects, especially for time series with nonzero mean. To avoid such effects, we have transformed all analyzed time series to zero mean value before applying the wavelet technique. A simplified expression of the Morlet function has the form

$$\psi(\tau) = \pi^{-1/4} \exp(j2\pi f_0 \tau) \exp\left[-\frac{\tau^2}{2} \right]. \tag{6}$$

The value f_0 allows us to search for a compromise between the localizations of the wavelet in the time and frequency domains. In our work, $f_0 = 1$ and 5. The relation between the scale a and the central frequency for the mother function f in this situation is $f = 1/a$.

Besides the coefficients $T_x(a,t)$, the energy density of the signal $x(t)$ in the time scale plane can be estimated: $E_x(a,t) \sim \mid T_x(a,t) \mid^2$. Following the definition used in [14], the coefficient of proportionality between $E_x(a,t)$ and $\mid T_x(a,t) \mid^2$ depends on both the scale and the shape of the mother wavelet, although in some works the simpler expression ($E_x(a,t) = \mid T_x(a,t) \mid^2$) is considered. Note that the moduli of the original wavelet coefficients $T_x(a,t)$ estimated from Eq. 1 do not correspond to actual amplitudes of the rhythmic components. To study amplitude variations, it is possible to slightly change the definition of the wavelet transform [18] or to make corrections for the energy density $E_x(a,t)$. In the present work we consider $E_x(a,t) = Ca^{-1} \mid T_x(a,t) \mid^2$, where C is a parameter that depends on the wavelet mother function.

3.1.2 Experimental Details

We have previously shown [41] that wavelet analysis reveals a range of frequencies in the refractive index dynamics of neurons. These frequencies result from the cooperative processes inside the cell. The processes that occur in different parts of the cell vary from compartment to compartment and so do the frequencies of the

local cellular dynamics. Moreover, different types of cells are also expected to exhibit different frequencies due to the distinction of their properties and processes. In this work we compare the dynamics of the refractive indices for excitable (neurons) and for non-excitable (mast cells and erythrocytes) cells. Neurons have the most active processes at the plasma membrane, and the local changes of the refractive index associated with these processes should exceed the changes observed for other cells. Mast cells represent a cell type with an active vesicular transport and exocytosis, whereas erythrocytes are simple cells with a dense packing of hemoglobin and a rigid submembrane structure. We shall consider the dynamics of the refractive index (RI) in the following regions of neurons and mast cells: in the membrane region, center region, and nucleus region (for mast cells only). As the volume ratio membrane/cytoplasm is higher for the membrane region than for the center, the contribution of the membrane and submembrane processes into the RI dynamics is also higher for the cell boundary. Hence, in the case of the membrane region we explore mainly membrane and submembrane processes while for the cellular center we observe both membrane and cytoplasmic processes. In the nucleus region we study RI changes occurring due to the simultaneous processes in the plasma membrane, cytoplasm and nucleus. In the experiments with erythrocytes we did not distinguish different cellular regions.

3.1.3 Neurons

Figure 6 shows power spectra of the refractive index changes in the neuron membrane (a, b) and center (c, d). Note that the low and high frequency bands are represented separately since different values of f_0 are used for their calculation ($f_0 = 1$ and $f_0 = 5$, respectively) and because the involved rhythmic components have very different powers. The peaks distinguished in the spectra are correlated to the rates of change in the refractive index during the observation time. It is seen that in the low frequency range (Figure 6a and c) the power of frequencies is higher in the plasma membrane region (a) than in the cell center (c). The spectral structure is similar for both regions. Thus, we suppose that low frequencies (0.1–6 Hz) correspond to processes taking place in the plasma membrane and submembrane regions. The low intensive frequencies in the cell center can be considered as the plasma membrane 'echo'. On the contrary, in the high frequency range (Figure 6c and d) the intensities are higher for the center than for the plasma membrane. The spectral structure is more complicated than for the low frequency range and differs slightly between the membrane and center regions. We suppose that the rhythms of cytoplasm processes lie in the region of high frequencies (6–20 Hz), so that they have higher power in the cell center than in the membrane region. The difference of the spectral structures for the examined cellular parts can be caused by the above-mentioned processes in the submembrane region. We should note that the spectral structure for leech neurons in general is very similar to that of snail neurons [41]. This points to a common origin of the spectral frequencies. Electrophysiological studies on the isolated mollusca neurons show that neurons display intrinsic electrical activity: (a) changes of the potential with 0.2–0.4 Hz frequencies caused by ion channel activity [42]; (b) intrinsic 1 and 1.5–3 Hz electric activity [43] and spontaneous firing with 1–10 Hz frequencies [44]. Hence, we suppose that the low frequency components of the RI dynamics correspond to the following membrane processes: (a) frequencies

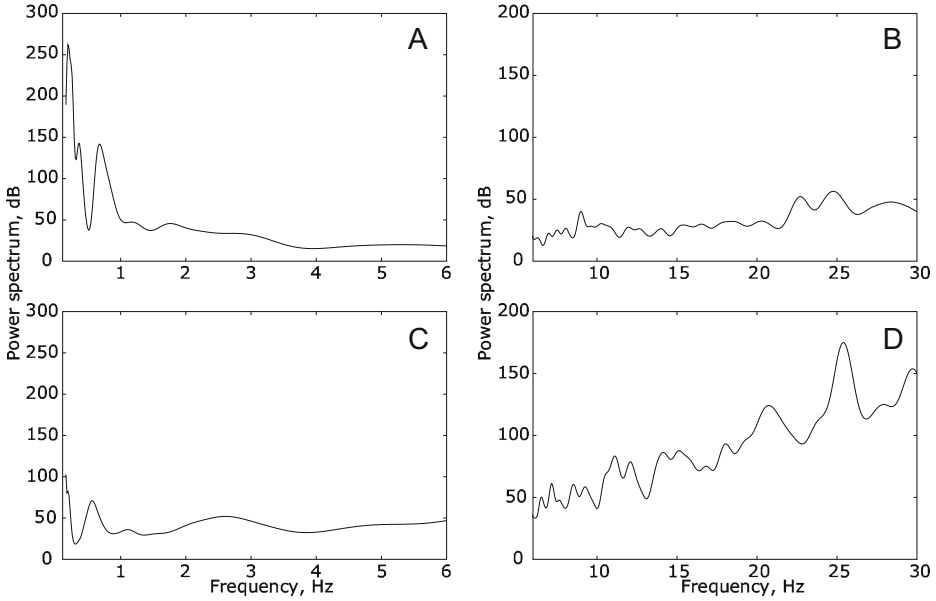

Figure 6 Power spectra calculated *via* the wavelet technique for the *low* (*left column*) and *high* (*right column*) frequency bands of the submembrane (**a**, **b**) and center (**c**, **d**) regions of neurons.

around 0.1 and 0.2–0.4 Hz originate from the complex reorganization in the plasma membrane (local fluctuations of the membrane fluidity and potential, lipid rafts and protein movements, activity of ion channels); (b) rhythms around 1 and 2–3 Hz relate to the subthreshold changes of the membrane potential and/or to spontaneous rhythmic activity. Landowne and Cohen [45] estimated frequencies of the light scattering changes from the synaptic terminals (8–40 Hz) and showed that the changes originated from the transport of synaptic vesicles. Based on this finding we suggest that rhythms in the high frequency range result from the movement of organelles (vesicles, mitochondria, etc.) and possibly also from cytoskeleton reorganization. In addition, spontaneous bursting activity of neurons may contribute to these rhythms [46].

3.1.4 Mast Cells

Figure 7 shows spectral properties of RI dynamics in the membrane region (a, b), center (c, d) and nucleus region (e, f) of a mast cell. Note that the Y-scale differs for the low and high frequency ranges. We immediately see that the spectral structures and power ratios of the frequencies in the membrane and center regions differ significantly from those observed for neurons. Rhythms around 1–2 Hz are broader than those for neurons, and peaks at 0.1–0.4 Hz, which have the highest power in neurons, are absent. Besides, mast cells possess a new rhythm around 4–6 Hz (Figures 6a, 7a). The power of the high frequency peaks in the membrane region of the mast cell essentially exceeds peak powers in the low frequency range (Figure 7a, b) The spectral structure in the center of the mast cells (Figure 7c, d) is similar to that of the membrane region, but the power of the main peaks is several times lower.

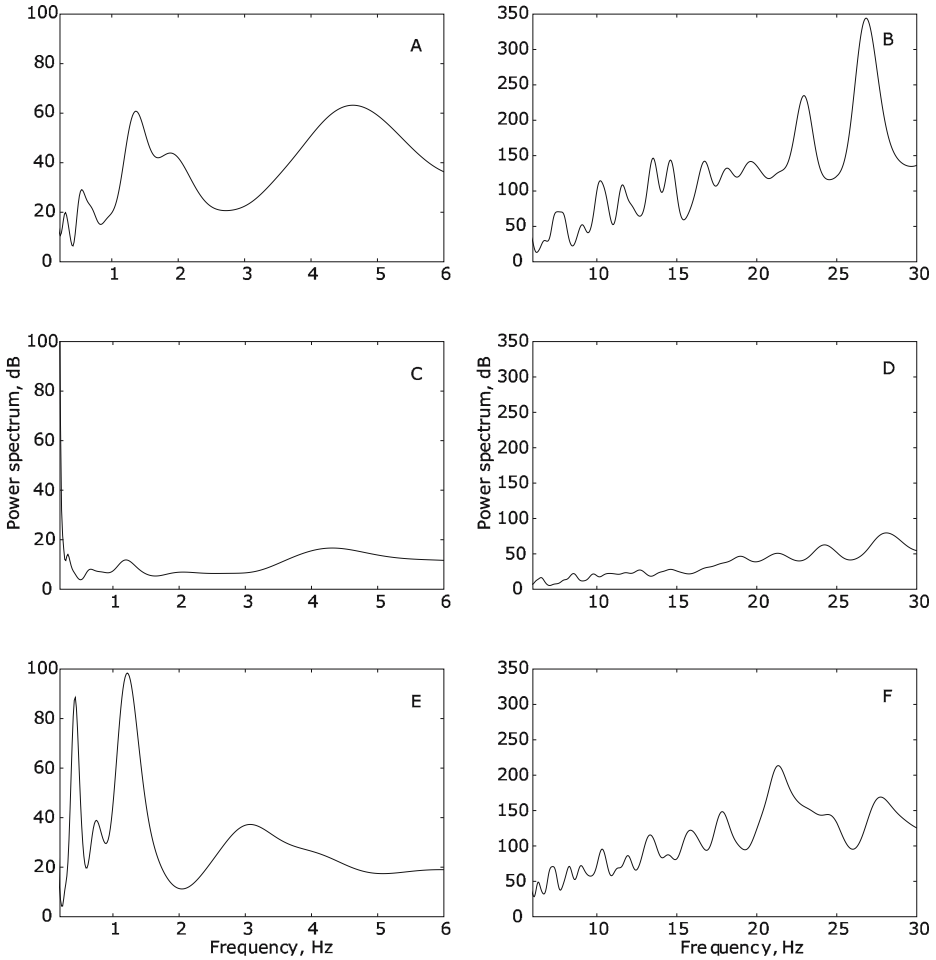

Figure 7 Power spectra calculated *via* the wavelet technique for the *low* (*left column*) and *high* (*right column*) frequency bands of the submembrane (**a**, **b**), center (**c**, **d**), and nucleus (**e**, **f**) regions of mast cells.

Therefore, we suppose that all frequencies observed in the membrane and center regions originate from processes in the plasma membrane and submembrane structures. The spectral structures for neurons and mast cells differ due to different plasma membrane and submembrane processes.

It is known that mast cells display active processes of vesicle transport and exocytosis [47–49]. We suggest that powerful rhythms with 24 and 26 Hz frequencies (Figure 7b) result from vesicle movements in the submembrane region, the fusion of the vesicles with the plasma membrane, and the subsequent exocytosis. Similar rhythms (22–25 Hz) are observed for neurons (Figure 6b, d) that also have transport of vesicles and exocytosis. This suggestion agrees with the data reported by Landowne and Cohen [45]. We suggest that the highest peaks in the power spectra belong to the most active cellular processes. As the most active processes in neurons

are related to changes in the membrane potential, the highest peaks in their spectra are rhythms around 0.1–0.4 and 1–2 Hz. For mast cells the major process is vesicle transport and exocytosis. Thus, the highest powers are associated with the rhythms at 24 and 26 Hz.

As noted, the low frequency spectra for the cellular center display lower powers than for the membrane and submembrane regions. This may be due the fact that the main changes of the refractive index occur in the cellular membranes while the intrinsic RI changes in the cytoplasm are relatively small or/and are averaged due to the large amount of cytoplasmic processes. Based on this assumption we expect the RI dynamics to be more intense in the regions with extended intracellular membranes. To examine this hypothesis we study RI dynamics in the nucleus region of the mast cells. It can be seen that the power of the main peaks in the low frequency range (Figure 7e, f) even exceeds the power in the membrane region, and the spectral structure differs slightly from structures observed in the other cellular regions. In the region of the nucleus we register RI dynamics from the mast cell membrane, cytoplasm, nucleus membrane and nucleus matrix. Thus, the spectrum from the nucleus region is a combination of rhythms that are characteristic for the plasma membrane, the center regions and the nucleus.

3.1.5 Erythrocytes

Figure 8 presents low (a) and high (b) frequency spectra for RI dynamics of erythrocytes. The spectral structure is different from the structure of neurons and mast cells, and the powers of the main peaks are lower. We suppose that this is due to the rigid submembrane and membrane structure that prevent strong changes in the membrane and cytoplasm and, therefore, eliminate visible changes of the refractive index. However, we believe that it is possible to register more pronounced RI dynamics using objectives with a higher aperture.

3.2 Modulation Processes under Double-wavelet Analysis

Processes in the cell are interrelated and influence one another. Due to this interaction, some of the observed frequencies of the RI dynamics can be non-stationary and

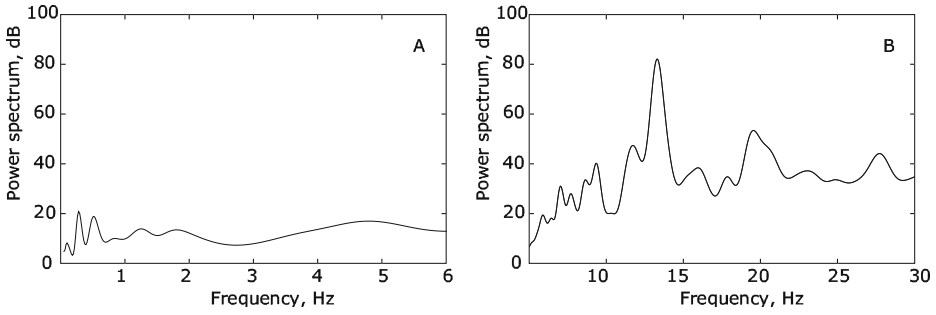

Figure 8 Power spectra calculated *via* the wavelet technique for erythrocytes at the *low* (**a**) and *high* (**b**) frequency bands.

modulated by other slower rhythms. Previously we found for neurons that rhythms between 0.1 and 0.3 Hz maintain constant values in time while rhythms between 1 and 2–4 Hz demonstrate variations caused by the slower components. In the high frequency range (10–20 Hz), there is a large number of coexisting rhythmic components with quite nonstationary behavior and different modulation properties [41].

Modulation of fast oscillations by slower dynamics can be considered as a form of nonlinear interaction between the involved modes, and this phenomenon may help to relate observed frequencies to particular cellular processes. Aiming to study modulation properties of the fast mode, we propose the use of the following approach [41]. The time-dependence of the instantaneous frequency $f_{fast}(t)$ is considered as input signal for the next wavelet transform (1). Again, the wavelet coefficients and the energy density are estimated and the simplified visualization of the energy density is considered. The latter will contain information about all modes involved in the modulation process. In the case of nonstationary dynamics we can examine how the features of the frequency modulation change in time. By analogy, instead of the instantaneous frequency of the fast dynamics we can take the instantaneous amplitude of this oscillatory mode and, in this way, it is possible to study the properties of amplitude modulation of the fast rhythm as well. This approach, which we shall refer to as a *double-wavelet analysis*, allows us to characterize the nonstationary temporal dynamics of a modulated signal, i.e., to detect all components that are involved in the modulation, estimate their contributions, and analyze whether the modulation properties change during the observation time.

We have previously investigated amplitude and frequency modulations of the neuronal rhythms at 1, 2–4, 11 and 17 Hz under normal conditions. We showed that these rhythms are well separated by their modulation frequencies and intensities of modulation [41]. Analysis of rhythm modulations can help to correlate observed frequencies with certain cellular processes. Besides, change of modulation can indicate change of the cellular processes. In the present work we consider the effect of KCl depolarization and of the K^+ ionophore valinomycin on the amplitude modulation of the neuronal 1 Hz rhythm. This frequency was chosen as a rhythm related to the dynamics of the membrane potential. We have analyzed the modulation of 1 Hz frequency in the plasma membrane and center regions of neurons. After the wavelet analysis of the amplitude dynamics of the 1 Hz rhythm, we obtained the spectra of amplitude modulation for the 1 Hz frequency. Usually, each spectrum of amplitude modulation has several peaks with one well-defined maximum (main frequency of modulation).

Figure 9 shows the distribution of main frequencies for the amplitude modulation of the 1 Hz rhythm in the plasma membrane region (a and b) and the center of the neuron (c and d). White dots correspond to the control (neurons in normal physiological solution), black dots correspond to the K-depolarization (exchange of the normal solution for a solution with increased K^+ concentration) (Figure 9a and c) or addition of valinomycin to the chamber with neurons (ultimate concentration: 1 μm) (Figure 9b and d). In the plasma membrane K^+-depolarization causes an increase in the intensity of modulation and shift of the main frequency of modulation to a lower frequency range. By contrast, addition of valinomycin results in a shift of the main frequency of modulation to the higher frequency range without change of the modulation intensity. The different effects of high K^+ concentration and valinomycin fit well with their influence on the membrane potential: the increased amount of

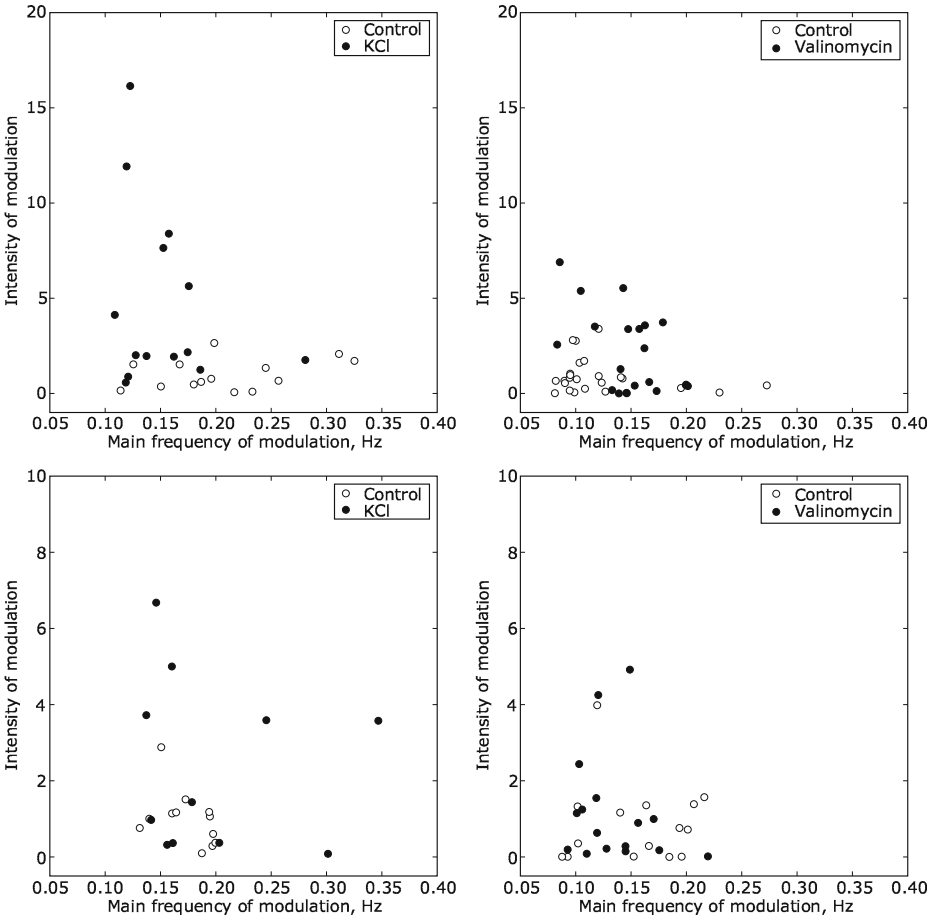

Figure 9 Distribution of the intensity and main modulation frequency for 1 Hz rhythm for isolated leech neurons in the case of amplitude modulation. (**a**), (**b**) correspond to the membrane region; (**c**), (**d**) correspond to the cell center. *White dots* corresponds to the control, *black dots* indicate the K^+-depolarization (**a**, **c**) or addition of valinomycin to the chamber containing the neurons (**b**, **d**).

K^+ causes the depolarization of plasma membrane, whereas valinomycin produces outward transport of K^+ ions and, hence, hyperpolarization. Based on these observations, we suggest that the modulation properties of the 1 Hz rhythm can serve as a marker of changes of the membrane potential. In the center of neurons neither high K^+ concentration nor valinomycin alter the modulation of the 1 Hz frequency (Figure 9c and d). This may be due either to the relatively low signal from the plasma membrane or to the absence of effects on the cytoplasm processes. These results confirm our suggestion about the origin of 1 Hz frequency as related to a change of plasma membrane properties (oscillations of the membrane potential). We suggest that rhythms of RI dynamics and their amplitude and frequency modulations can be used for additional information about the cell properties and effect of various stimuli.

4 Summary

In this paper we demonstrated how interference microscopy combined with advanced wavelet analysis can be used for non-invasive studies of cellular dynamics and for cell visualization. We showed that interference microscopy can be applied to investigations of different cell types, not only excitable cells, but also non-excitable, such as erythrocytes and mast cells. Interference images of cells provide new data about their compartmentalization, membrane and submembrane structures at normal conditions and under influence of stimuli (chemicals, drugs, etc.). We found, for instance, that interference images of erythrocytes can reveal changes of cytoskeleton structure and hemoglobin distribution that can hardly be observed by traditional optical microscopy. We demonstrated that K^+-depolarization alters the interference images of neurons. Thus, interference microscopy can be applied for studies of ions' and neurotransmitters' effects on nerve cells.

We also studied the dynamics of the refractive index in different cell types: neurons, mast cells and erythrocytes. We showed that the RI dynamics differs among the studied cells and depends on the cellular compartment. We propose that (a) low frequency dynamics in neurons and mast cells relates to processes in the plasma membrane and submembrane regions (e.g., change of the physical-chemical properties of the plasma membrane); (b) well-distinguished high frequencies (e.g., 24 and 26 Hz for mast cells) correspond to vesicular transport. Using double-wavelet analysis we demonstrated that the 1 Hz rhythm in neurons depends on the membrane potential and that its amplitude modulation changes in opposite ways under depolarization and hyperpolarization of the plasma membrane. Based on this finding we suggest that the 1 Hz rhythm can be used for studies of changes of the membrane potential. This can be important for investigation of the electric properties of small neurons, glial cells and tiny nerve fibers that cannot be studied by traditional microelectrode techniques.

Interference cell imaging and investigation of cellular dynamics with wavelet analysis are promising to approaches for non-invasive cell studies, for cell visualization, and for the unravelling of the relations between different spatial and temporal processes under normal and pathological conditions.

Acknowledgements This work was partly supported by the European Union through the Network of Excellence BioSim, Contract No. LSHB-CT-2004-005137). We acknowledge the company 'Amphora Laboratories' (http://www.amphoralabs.ru) for providing the laser interference microscope MIM-2.1. We are thankful to Dr Dmitriy Orlov for the excellent technical assistance during the experiments. We are grateful to Drs Oleg Rodnenkov, Medeya Akhalaya and Elizaveta Graevskaya for providing cell samples. N.B., A.B. and L.E. acknowledge support from Moscow Government, N.B. acknowledges support from Government of Russian Federation, and AB acknowledges support from President of Russian Federation.

References

1. Hill D.K., Keynes R.D.: Opacity changes in stimulated nerve. J. Physiol. (London) **108**, 278–281 (1949)
2. Hill, D.K.: The effect of stimulation on the opacity of crustacean nerve. J. Physiol. (London) **111**, 283–303 (1950)
3. Cohen, L.B., Keynes, R.D., Hille, B.: Light scattering and birefringence changes during nerve activity. Nature **218**, 438–441 (1968)

4. Stepnoski, R.A., LaPorta, A., Raccuia-Behling, F., Blonder, J.E., Slusher, R.E., Kleinfeld, D.: Noninvasive detection of changes in membrane potential in cultured neurons by light scattering. Proc. Nat. Acad. Sci. USA **88**, 9382–9386 (1991)
5. Haller, M., Mironov, S.L., Richter, D.W.: Intrinsic optic signals in respiratory brain stem regions of mice: neurotransmitters, neuromodulators, and metabolic stress. J. Neurophysiol. **86**, 412–421 (2001)
6. Boppart, S.A.: Optical coherence tomography: technology and application for neuroimaging. Psychophysiology **40**, 529–541 (2003)
7. Lazebnik, M., Marks, D.L., Potgieter, K.L., Gillete, R., Boppart, S.A.: Functional optical coherence tomography for detecting neural activity through scattering changes. Opt. Lett. **28**, 1218–1220 (2003)
8. Kleinfeld, D., LaPorta, A.: Detection of action potentials *in vitro* by changes in refractive index. In: Light Scattering Imaging of Neural Tissue Function. Humana Press, Totowa, New Jersey (2003)
9. Maksimov, G.V., Nikandrov, S.L., Lazareva, E.S., Tychinskii, V.P., Rubin, A.B.: A study of demyelination of nerve fibers using dynamic phase contrast microscopy. Bull. Exp. Biol. Med. **131**, 457–460 (2001)
10. Brazhe, N.A., Erokhova, L.A., Churin, A.A., Maksimov, G.V.: The relation of different-scale membrane processes under nitric oxide influence. J. Biol. Phys. **31**, 531–546 (2005)
11. Wolf, M.M., Varigos, G.A., Hunt, D., Sloman, J.G.: Sinus arrhythmia in acute myocardial infarction. Med. J. Aust. **2**, 52–53 (1978)
12. Grossmann, A., Morlet, J.: Decomposition of Hardy functions into square integrable wavelets of constant shape. S.I.A.M. J. Math. Anal. **15**, 723–736 (1984)
13. Daubechies, I.: Ten Lectures on Wavelets, S.I.A.M., Philadelphia (1992)
14. Kaiser, G.: A Friendly Guide to Wavelets. Boston, Birkhäuser (1994)
15. Grossmann, A., Kronland-Martinet, R., Morlet, J.: In: Combes et al. (eds.) Wavelets: Time-Frequency Methods and Phase Space. Springer, Berlin (1989)
16. Quian Quiroga, R., Kraskov, A., Kreuz, T., Grassberger, P.: Performance of different synchronization measures in real data: a case study on electroencephalographic signals. Phys. Rev. E **65**, 041903-1-14 (2002)
17. Peng, C.K., Havlin, S., Stanley, H.E., Goldberger, A.L.: Quantification of scaling exponents and crossover phenomena in nonstationary heartbeat time series. Chaos **5**, 82–87 (1995)
18. Muzy, J.F., Bacry, E., Arneodo, A.: The multifractal formalism revisited with wavelets. Int. J. Bifurc. Chaos **4**, 245–302 (1994)
19. Braun, H.A., Bade, H., Hensel, H.: Static and dynamic discharge patterns of bursting cold fibers related to hypothetical receptor mechanisms. Pflügers Arch. **386**, 1 (1980)
20. Goldbeter, A.: Biochemical Oscillations and Cellular Rhythms. Cambridge University Press, Cambridge, UK (1996)
21. Tass, P., Rosenblum, M.G., Weule, J., Kurths, J., Pikovsky, A., Volkmann, J., Schnitzler, A., Freund, H.J.: Phys. Rev. Lett. **81**, 3291–3294 (1998)
22. Chon, K.H., Chen, Y.M., Marmarelis, V.Z., Marsh, D.J., Holstein-Rathlou, N.-H.: Detection of interactions between myogenic and tgf mechnisms using nonlinear analysis. Amer. J. Phys. **267**, F160–F173 (1994) (Renal Fluid Electrolyte Physiol. 36)
23. Sosnovtseva, O.V., Pavlov, A.N., Mosekilde, E., Holstein-Rathlou, N.-H.: Bimodal oscillations in nephron autoregulation. Phys. Rev. E **66**, 061909-1-7 (2002)
24. Pikovsky, A., Rosenblum, M., Kurths, J.: Synchronization: A Universal Concept in Nonlinear Sciences. Cambridge Nonlinear Science Series 12, Cambridge University Press, Cambridge, UK (2001)
25. Mosekilde, E., Maistrenko, Y., Postnov, D.: Chaotic Synchronization: Applications to Living Systems. World Scientific, Singapore (2002)
26. Sosnovtseva, O.V., Pavlov, A.N., Mosekilde, E., Holstein-Rathlou, N.-H., Marsh, D.J.: A double-wavelet approach to study frequency and amplitude modulation in renal autoregulation. Phys. Rev. E **70**, 031915-1-8 (2004)
27. Tychinskii, V.P., Kufal', G.E., Vyshenskaya, T.V., Perevedentseva, E.V., Nikandrov, S.L.: Measurements of submicron structures with the airyscan laser phase microscope. Quantum Elec. **27**, 735–739 (1997)
28. Tychinskii, V.P.: Coherent phase microscopy of intracellular processes. Phys. Uspekhi **44**, 683–696 (2001)

29. Maksimov, G.V., Brindikova, T.A., Erokhova, L.A., Kleinhauz, A.L., Rubin, A.B.: Redistribution of membrane-bound Ca^{2+} in neurolemma of leech Retzius-neurons during thermostimulation. Biophysics **48**, 683–689 (2003)
30. Brandon, D., Kaplan, W.D.: Microstructural Characterization of Materials. Wiley, Chichester, West Sussex, UK (1999)
31. Andreev, V.A., Indukaev, K.V.: The problem of subrayleigh resolution in interference microscopy. J. Russ. Laser Res. **24**, 220–236 (2003)
32. Andreev, V.A., Indukaev, K.V.: Phase modulation microscope MIM-2.1 for measurements of surface microrelief. General principles of design and operation. J. Russ. Laser Res. **26**, 380–393 (2005)
33. Erokhova, L.A., Novikov, S.M., Lazarev, G.L., Kazakova, T.A., Orlov, D.A., Indukaev, K.V., Maksimov, G.V.: Study of regular intracellular and membrane processes in neurons by laser interference microscopy. Bull. Exp. Biol. Med. **140**, 262–264 (2005)
34. Graevskaya, E.E., Akhalaya, M.Y., Goncharenko, E.N.: Effects of cold stress and epinephrine on degranulation of peritoneal mast cells in rats. Bull. Exp. Biol. Med. **131**, 333–335 (2001)
35. Ul'ianova, N.A., Maksimov, G.V., Churin, A.A., Rubin, A.B.: Effect of nitric oxide on viscosity of nerve cell membranes. Biophysics **50**, 289–296 (2005)
36. Rodnenkov, O.V., Luneva, O.G., Ulyanova, N.A., Maksimov, G.V., Rubin, A.B., Orlov, S.N., Chazov, E.I.: Erythrocyte membrane fluidity and haemoglobin haemoporphyrin conformation: features revealed in patients with heart failure. Pathophysiology **11**, 209–213 (2005)
37. Luneva, O.G., Brazhe, N.A., Fadyukova, O.E., Akhalaya, M.Ya., Baizhumanov, A.A., Parshina, E.Yu., Demidova, A.E., Koshelev, V.B., Maksimov, G.V.: Changes in plasma membrane viscosity and hemoporphyrin conformation in erythrocyte hemoglobin under the conditions of ischemia and reperfusion of rat brain. Dokl. Biochem. Biophys. **405**, 465–468 (2005)
38. Hille, B.: Ion Channels of Exitable Membranes. Sinauer Associates, Sunderland, Mass (1992)
39. Metuzuls, J., Montpetit, V., Clapin, D.F.: Organization of the neurofilamentous network. Cell Tissue Res. **214**, 455–482 (1981)
40. Mironov, S.L., Ivannikov, M.V., Johansson, M.: $[Ca^{2+}]_i$ signaling between mitochondria and endoplasmic reticulum in neurons is regulated by microtubules: from mitochondrial permeability transition pore to Ca^{2+}-induced Ca^{2+} release. J. Biol. Chem. **280**, 715–721 (2005)
41. Sosnovtseva, O.V., Pavlov, A.N., Brazhe, N.A., Brazhe, A.R., Erokhova, L.A., Maksimov, G.V., Mosekilde, E.: Interference microscopy under double-wavelet analysis: a new approach to studying cell dynamics. Phys. Rev. Lett. **94**, 218103-1-4 (2005)
42. Szucs, A., Molnar, G., S-Rozsa, K.: Periodic and oscillatory firing patterns in identified nerve cells of *Lymnaea Stagnalis L.*, Acta Biol. Hung. **50**, 269–278 (1999)
43. Schutt, A., Bullock, T.H., Basar, E.: Odor input generates 1.5 Hz and 3 Hz spectral peaks in the *Helix* pedal ganglion. Brain Res. **879**, 73–87 (2000)
44. Cohen, L.B.: Changes in neuron structure during action potential propagation and synaptic transmission. Physiol. Rev. **53**, 373–418 (1973)
45. Landowne, D., Cohen, L.B.: Changes in light scattering during synaptic activity in the electric organ of the skate, *Raia Erinacea*. Biol. Bull. **137**, 407–408 (1969)
46. Reboreda, A., Sanchez, E., Romero, M., Lamas, J.A.: Intrinsic spontaneous activity and subthreshold oscillations in neurones of the rat dorsal column nuclei in culture. J. Physiol. **551**, 191–205 (2003)
47. Dvorak, A.M.: Basophil and Mast Cell Degranulation and Recovery. Plenum, New York (1991)
48. Abraham, S.N., Malaviya, R.: Mast cells in infection and immunity. Infect. Immun. **65**, 3501–3508 (1997)
49. Logan, M.R., Odemuyiwa, S.O., Moqbel, R.: Understanding exocytosis in immune and inflammatory cells: the molecular basis of mediator secretion. J. Allergy Clin. Immunol. **111**, 923–932 (2003)